SYMBOL TIMING RECOVERY FOR SOQPSK

Prashanth Chandran
Department of Electrical Engineering and Computer Science
University of Kansas
Lawrence, KS 66046
chandran@ittc.ku.edu

Faculty Advisor:
Erik Perrins

ABSTRACT

Shaped offset quadrature phase shift keying (SOQPSK) is a highly bandwidth efficient modulation technique used widely in military and aeronautical telemetry standards. It can be classified as a form of continuous phase modulation (CPM), but its major distinction from other CPM schemes is that it has a constrained (correlated) ternary data alphabet. CPM-based detection models for SOQPSK have been developed only recently. One roadblock standing in the way of these detectors being adopted is that existing symbol timing recovery techniques for CPM are not always applicable since the data symbols are correlated. We investigate the performance of one CPM-based timing error detector (TED) that can be used with SOQPSK, and apply it to the versions of SOQPSK used in military (MIL-STD SOQPSK) and telemetry group (SOQPSK-TG) standards. We derive the theoretical performance limits on the accuracy of timing recovery for SOQPSK, as given by the modified Cramer-Rao bound (MCRB), and show that the proposed TED performs close to these bounds in computer simulations and is free of false-lock points. We also show that the proposed scheme outperforms a non-data aided TED that was recently developed for SOQPSK. These results show that the proposed scheme has great promise in a wide range of applications due to its low complexity, strong performance, and lack of false-lock points.

I. INTRODUCTION

Shaped-offset quadrature phase shift keying (SOQPSK) is a highly bandwidth efficient form of continuous phase modulation (CPM) [1] based on a constrained (correlated) ternary data alphabet. Its constant-envelope nature makes it transmitter-friendly in terms of its compatibility with non-linear amplifiers and their efficiency in converting limited (e.g. battery) power into radiated power. In spite of its advantages on the transmit side, CPM typically suffers from high complexity and synchronization problems on the receive side.

There are two versions of SOQPSK in current use. Military-standard (MIL-STD) SOQPSK [2] is the original and simplest version; it uses a rectangular shaped frequency pulse that spans a single bit time (full-response) and can be described by a trellis (state machine) with 4 states. A more complicated version has been adopted recently by the aeronautical telemetry group (SOQPSK-TG) [3]; this more bandwidth-

efficient version has a frequency pulse that spans eight bit times (partial-response) and can be described by a trellis (state machine) with 512 states.

In this paper, we address the problem of timing synchronization for SOQPSK. As its name suggests, SOQPSK shares a number of similarities with traditional OQPSK. In fact, until recently, the typical receiver model for SOQPSK has always been a suboptimal OQPSK-type detector and suboptimal OQPSK-type synchronization techniques [4]. The downside of OQPSK-type detection is that it ignores the inherent state memory of the signal and is not truly *matched* to the transmitted waveform; a performance penalty of 1–2 dB results with symbol-by-symbol OQPSK detection. The shortcomings of OQPSK-type detection have been addressed recently with a cross-correlated trellis quadrature coded modulation (XTCQM) approach in [5] and a CPM-based approach in [6]; both of these recent approaches yield optimal 4-state *trellis-based* detectors for MIL-STD SOQPSK that outperform OQPSK-type detection by 1–2 dB. Furthermore, the CPM-based approach is compatible with powerful CPM complexity reduction techniques, such as the pulse amplitude modulation (PAM) approximation [7, 8] and frequency pulse truncation (PT) technique [9, 10]; these techniques have allowed 4-state detectors for SOQPSK-TG to perform within 0.1 dB of the optimal 512 state detector [11]. Future applications of CPM-based detectors include *noncoherent sequence detection* schemes, e.g. [12], which are of interest for their robustness in operating environments where fully coherent detection is ineffective.

None of the above mentioned detectors can be realized without symbol timing recovery schemes; thus, the techniques developed here are highly motivated and timely. The contributions of this paper are the following:

- Adapt an existing CPM-based timing error detector (TED) [13] so that the constrained ternary nature of CPM is properly taken into account.
- Incorporate the TED into the Viterbi algorithm (VA) based SOQPSK detectors and properly combine it with the 4-state PT technique.
- Compute the modified Cramer-Rao bound (MCRB), which establishes the theoretical performance limits on the accuracy (normalized variance) of timing recovery for SOQPSK.
- Quantify the performance of the timing recovery scheme in computer simulations; we compare normalized variance vs. MCRB, and bit error rate (BER) vs. theoretical probability of errror.

The proposed scheme is shown to have extremely low complexity, low normalized variance that approaches the MCRB, and is free of false lock points. As such, it is an attractive solution to the timing recovery problem for CPM-based SOQPSK detectors.

The paper is organized as follows. In Section II we describe the signal model. In Section III we derive the TED using maximum-likelihood methods and making some minor modifications to the existing one. In Section IV we establish the lower bound on the performance of the proposed approach by computing the MCRB, and in Section V we give numerical results.

II. SIGNAL MODEL

The complex-baseband SOQPSK signal model begins with the standard CPM signal, which is defined as [1]

$$s(t,\boldsymbol{\alpha}) \triangleq \sqrt{\frac{E_s}{T_s}} \exp\{j\phi(t,\boldsymbol{\alpha})\} \tag{1}$$

where E_s is the symbol energy and T_s is the symbol duration. The phase is a pulse train of the form

$$\phi(t,\boldsymbol{\alpha}) \triangleq 2\pi h \sum_i \alpha_i q(t-iT_s) \tag{2}$$

where $i \in \mathbb{Z}$ is the discrete-time index, $\boldsymbol{\alpha} \triangleq \{\alpha_i\}$ is the sequence of M-ary data symbols, and h is the modulation index. The *phase pulse* $q(t)$ is defined as

$$q(t) \triangleq \begin{cases} 0 & t < 0 \\ \displaystyle\int_0^t g(\sigma)\, d\sigma & 0 \le t < LT_s \\ 1/2 & t \ge LT_s \end{cases} \tag{3}$$

where $g(t)$ is the *frequency pulse* which has a duration of L symbol times and an area of 1/2.

The phase $\phi(t,\boldsymbol{\alpha})$ in (2) can be expressed as

$$\begin{aligned} \phi(t,\boldsymbol{\alpha}) &= \eta(t,\boldsymbol{C}_k,\alpha_k) + \boldsymbol{\phi}_k, \\ &\qquad kT_s \leqslant t < (k+1)T_s \end{aligned} \tag{4}$$

with

$$\eta(t,\boldsymbol{C}_k,\alpha_k) \triangleq 2\pi h \sum_{i=k-L+1}^{k} \alpha_i q(t-iT_s) \tag{5}$$

$$\boldsymbol{C}_k \triangleq (\alpha_{k-L+1}, ..., \alpha_{k-2}, \alpha_{k-1}) \tag{6}$$

$$\tag{7}$$

and

$$\boldsymbol{\phi}_k \triangleq \pi h \sum_{i=0}^{k-L} \alpha_i \mod 2\pi. \tag{8}$$

In the above equations $\boldsymbol{C}_k$ is the *correlative state*, α_k is the *current symbol*, and $\boldsymbol{\phi}_k$ is the *phase state* of the modulator.

The different versions of SOQPSK have different frequency pulse shapes. The original version of SOQPSK, known as "MIL-STD" SOQPSK [2], uses a full-response ($L = 1$) rectangular frequency pulse (1REC). A version of SOQPSK recently adopted in aeronautical telemetry, known as "SOQPSK-TG," uses a partial-response ($L > 1$) frequency pulse shape defined in [3]. The modulation index for all versions of SOQPSK is $h = 1/2$.

The transmitted symbols $\{\alpha_i\}$ are derived from a sequence of i.i.d. information symbols $\{u_i\}$ by a *precoding* operation [14]

$$\alpha_i(\boldsymbol{u}) \triangleq \frac{1}{2}(-1)^{i+1} u_{i-1}(u_i - u_{i-2}) \tag{9}$$

where $u_i \in \{\pm 1\}$ and $\alpha_i \in \{-1, 0, +1\}$. The reason for this non-obvious precoding operation is that (9) orients the phase of the CPM signal in (2) such that it behaves like the phase of an OQPSK signal that is driven by the i.i.d. bit sequence $\boldsymbol{u}$. In fact, $\boldsymbol{u}$ can be recovered directly from the received signal, with no additional steps, by a suboptimal symbol-by-symbol OQPSK-type detector [4, 15]. For convenience, we use the notation α_i instead of $\alpha_i(\boldsymbol{u})$, but we stress that $\boldsymbol{u}$ is the underlying information sequence for SOQPSK.

The SOQPSK precoder imposes three important constraints on the ternary data [14]:

1. While α_i is viewed as being *ternary*, in any given bit interval α_i is actually drawn from one of two *binary* alphabets, $\{0, +1\}$ or $\{0, -1\}$.

2. When $\alpha_i = 0$, the binary alphabet for α_{i+1} switches from the one used for α_i, when $\alpha_i \neq 0$ the binary alphabet for α_{i+1} does not change.

3. A value of $\alpha_i = +1$ cannot be followed by $\alpha_{i+1} = -1$, and vice versa (this is implied by the previous constraint).

Based on these constraints, the autocorrelation function for the SOQPSK symbol sequence $\boldsymbol{\alpha}$ is [16]

$$R_{\boldsymbol{\alpha}}(l) \triangleq \mathrm{E}\{\alpha_i \alpha_{i+l}\} = \begin{cases} 1, & l = 0 \\ \frac{1}{2}, & |l| = 1 \\ 0 & \text{otherwise.} \end{cases} \tag{10}$$

The above constraints also imply that not every possible ternary symbol pattern is a valid SOQPSK data pattern. For example, the ternary symbol sequences $..., 0, +1, -1, 0, ...$ and $\ldots, +1, 0, +1, \ldots$ violate the SOQPSK constraints.

In what follows, we refer to estimated and hypothesized values of a generic quantity x as $\hat{x}$ and $\tilde{x}$, respectively. Also, $\hat{x}$ and $\tilde{x}$ can assume the same values as x itself.

III. TIMING ERROR DETECTOR

The derivation of the timing error detector (TED) is based on maximum likelihood principles. The signal observed at the receiver is modeled as

$$r(t) = \sqrt{\frac{E_s}{T_s}} e^{j\phi(t-\tau, \boldsymbol{\alpha})} + w(t)$$

where $w(t)$ is complex-valued additive white Gaussian noise (AWGN) with zero mean and single-sided power spectral density N_0. The variables $\boldsymbol{\alpha}$ and τ represent the data symbols and timing offset, respectively, which are both unknown to the receiver in practice.

The operation of the TED is intertwined with the operation of the Viterbi algorithm (VA). Customarily, CPM signals are demodulated using a bank of M^L matched filers (MFs). But, in the case of SOQPSK it is important to note that though the original underlying data is binary, the precoding operation produces a ternary output and hence the MF bank for full-response SOQPSK is made of an array of three filters matched to $\{-1, 0, 1\}$. By applying the PT approximation [9, 10], it was shown in [11] that the same three MFs can be used for partial-response SOQPSK-TG.

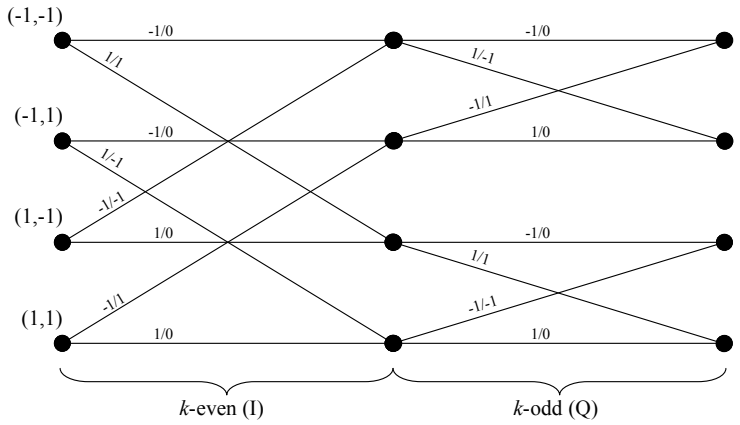

Figure 1: Four state trellis diagram for SOQPSK.

In order to obtain the sampled MF outputs, we assume for the moment that τ is known. The MF outputs are sampled at $\tau + (k+1)T_s$ to produce

$$\boldsymbol{Z}_k(\boldsymbol{C}_k, \alpha_k, \tau) \triangleq \int_{\tau+kT_s}^{\tau+(k+1)T_s} r(t) e^{-j\eta(t-\tau, \boldsymbol{C}_k, \alpha_k)} dt. \tag{11}$$

The likelihood function of the data is maximized by performing maximum likelihood sequence detection (MLSD), which is implemented efficiently via the VA. The sampled MF outputs $\boldsymbol{Z}_k$ are used to compute the branch metrics within the VA. The trellis of an SOQPSK modulated signal is shown in Fig. 1. The state variables in the trellis are taken from (9), and are ordered (u_{k-2}, u_{k-1}) for k-even and (u_{k-1}, u_{k-2}) for k-odd [14]; thus, the trellis states are $S_n \in \{(-1,-1), (-1,+1), (+1,-1), (+1,+1)\}$. The branches in Fig. 1 are labeled with the current-bit/current-symbol pair, u_k/α_k, for the given branch. The time-varying nature of the trellis is a result of the time-dependence in (9). The remainder of the details needed to implement the VA are found in [11].

In order to obtain the TED update, we temporarily assume that $\boldsymbol{\alpha}$ is known. Using the above definitions, and denoting the observation interval as $0 \le t \le L_0 T$, it can be shown that the likelihood function for the unknown parameter $\tilde{\tau}$ is

$$\Lambda(\boldsymbol{r}|\tilde{\tau}) = \exp\left\{ \frac{1}{N_0} \sqrt{\frac{E_s}{T_s}} \sum_{k=0}^{L_0-1} \text{Re}\left\{ \boldsymbol{Z}_k(\boldsymbol{C}_k, \alpha_k, \tilde{\tau}) e^{-j\boldsymbol{\phi}_k} \right\} \right\}. \tag{12}$$

The maximum of $\Lambda(\boldsymbol{r}|\tilde{\tau})$ with respect to the timing offset estimate $\tilde{\tau}$ is obtained by setting equal to zero the partial derivative of (12) with respect to $\tilde{\tau}$. Thus, we now have

$$\sum_{k=0}^{L_0-1} \text{Re}\left\{ \boldsymbol{Y}_k(\boldsymbol{C}_k, \alpha_k, \tilde{\tau}) e^{-j\boldsymbol{\phi}_k} \right\} = 0 \tag{13}$$

where $\boldsymbol{Y}_k$ is the derivative of $\boldsymbol{Z}_k$ with respect to $\tilde{\tau}$. A discrete-time differentiator is used to implement $\boldsymbol{Y}_k$, as discussed in Section V.

The solution to (13) is obtained in an adaptive/iterative manner. As it is formulated, (13) assumes the true data sequence $\{..., \alpha_{k-2}, \alpha_{k-1}, \alpha_k\}$ is known, which is not the case in practice. A logical substitute

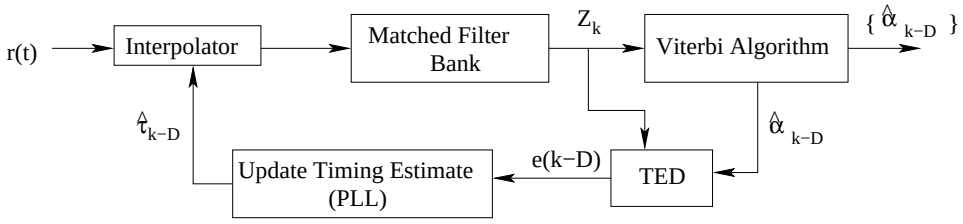

Figure 2: Block diagram of the final TED.

for the true data sequence is the sequence of survivors within the VA, which become more reliable the further we trace back along the trellis. Considering all these issues, the following error signal is obtained as in [13]

$$e(k-D) \triangleq \text{Re}\left\{ \boldsymbol{Y}_{k-D}(\boldsymbol{C}^b_{k-D}, \alpha^b_{k-D}, \hat{\tau}_{k-D}) e^{-j\phi^b_{k-D}} \right\} \tag{14}$$

where D is the traceback time for computing the error and the superscript b represents the best survivors of the VA. A large D could result in longer delays in the timing recovery loop, but it is observed in [13] and Section V that $D = 1$ produces satisfactory results.

A discrete-time implementation of (14) is shown in block diagram form in Fig. 2.

IV. MODIFIED CRAMER-RAO BOUND

We use the modified Cramer-Rao bound (MCRB) [17] to establish a lower bound on the degree of accuracy to which τ can be estimated for SOQPSK. Following the approach in [18, Ch. 2] the complete complex-baseband signal model is represented as

$$s(t, \tau, \boldsymbol{\alpha}) = \sqrt{\frac{E_s}{T_s}} e^{j\phi(t-\tau, \boldsymbol{\alpha})}. \tag{15}$$

The MCRB with respect to τ for a baseband signal is [18]

$$\text{MCRB}(\tau) = \frac{N_0/2}{\text{E}_{\boldsymbol{\alpha}}\left\{ \int_0^{T_0} \left| \dfrac{\partial s(t, \tau, \boldsymbol{\alpha})}{\partial \tau} \right|^2 dt \right\}} \tag{16}$$

where $T_0 \triangleq L_0 T_s$. Next, using the signal model in (15), we get

$$\text{E}_{\boldsymbol{\alpha}}\left\{ \int_0^{T_0} \left| \frac{\partial s(t, \tau, \boldsymbol{\alpha})}{\partial \tau} \right|^2 dt \right\} = \frac{4\pi^2 h^2 E_s}{T_s} \int_0^{T_0} G(t, \tau)\, dt$$

where

$$\begin{aligned} G(t, \tau) &\triangleq \text{E}_{\boldsymbol{\alpha}}\left\{ \left| \sum_i \alpha_i g(t - iT_s - \tau) \right|^2 \right\} \\ &= \sum_i \sum_l R_{\boldsymbol{\alpha}}(l) g(t - iT_s - \tau) g(t - [i+l]T_s - \tau) \end{aligned} \tag{17}$$

and $R_{\boldsymbol{\alpha}}(l)$ is the autocorrelation function of the sequence $\boldsymbol{\alpha}$.

At this point, the solution can be expressed in closed-form for MIL-STD SOQPSK using (10). In this case, (17) simplifies to

$$G_{\text{MIL}}(t,\tau) = 2\sum_i g^2(t - iT_s - \tau) \tag{18}$$

where only the $l = 0$ term is non-zero due to the brief duration of $g(t)$ (full-response, $L = 1$). After evaluating (18), the final result for MIL-STD SOQPSK is

$$\frac{1}{T_s^2} \times \text{MCRB}_{\text{MIL}}(\tau) = \frac{4}{\pi^2 L_0} \times \frac{1}{E_s/N_0}. \tag{19}$$

For SOQPSK-TG, a similar closed-form equation does not exist due to the shape of $g(t)$ which is a partial-response pulse with $L = 8$. But, (17) can be computed numerically with ease. Using (10) it is seen that only the $l = 0$ and $l = \pm 1$ terms will be non-zero as the correlation is zero for $l > 1$. Hence, for SOQPSK-TG (17) can be simplified as

$$G_{\text{TG}}(t,\tau) = 2\sum_i g^2(t - iT_s - \tau) + 2\sum_i g(t - iT_s - \tau)g(t - (i+1)T_s - \tau) \tag{20}$$

Once (20) is evaluated, the final result for SOQPSK-TG is

$$\frac{1}{T_s^2} \times \text{MCRB}_{\text{TG}}(\tau) = \frac{2}{\pi^2 L_0} \times \frac{1}{\int_0^{T_0} G_{\text{TG}}(t,\tau)dt} \times \frac{1}{E_s/N_0}. \tag{21}$$

V. NUMERICAL RESULTS

We now quantify the accuracy of the TED in Fig. 2 for the two versions of SOQPSK. The discrete-time implementation is sampled at a rate of $N = 4$ samples per symbol. Samples of $\boldsymbol{Z}_k$ are used to update the branch metrics within the VA. In addition to the sample used in the VA, an *early* sample of $\boldsymbol{Z}_k$ is taken, as well as a *late* sample. The difference between the early and late samples is used to approximate the derivative $\boldsymbol{Y}_k$. This procedure is discussed in [13].

The raw TED output $e[k]$ is refined into a more stable timing estimate $\hat{\tau}$ using a feedback scheme. A standard first-order phase-locked loop (PLL) provides an updated timing estimate after each symbol time with the operation

$$\hat{\tau}[k] \triangleq \hat{\tau}[k-1] + \gamma e[k]$$

where the *step size* is

$$\gamma \triangleq \frac{4}{k_p B T_s}$$

and BT_s is the user-specified *normalized loop bandwidth*.

The constant k_p is obtained from the S-curve of the TED; this curve characterizes the overall behavior of the TED and is the expected value of the TED output $e[k]$ as a function of the *timing offset*

$$\delta \triangleq \tau - \hat{\tau}.$$

The S-curve is particularly useful since it identifies the stable lock points for the TED; these are the zero-crossing points on the curve where the slope is positive, e.g. [18]. In this case, a closed-form expression for the expected value of $e[k]$ does not exist and we instead use simulations to study the S-curve. The simulations reveal that the only stable lock point occurs when the timing is correct, i.e. at $\delta = 0$. This

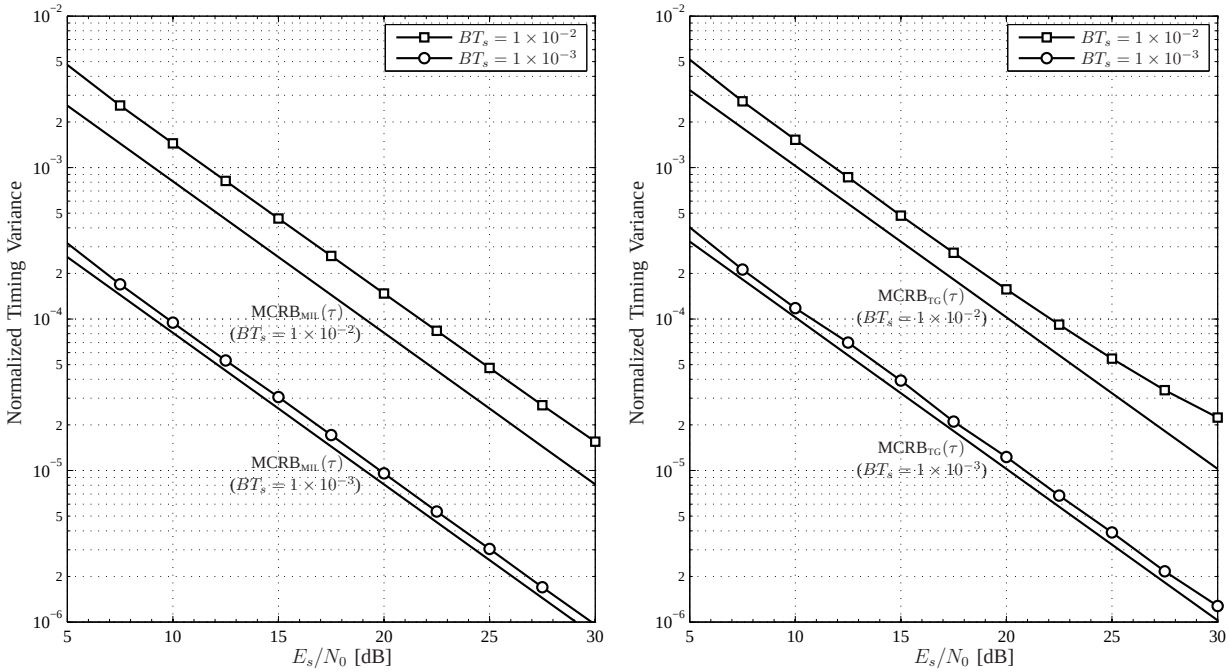

(a) (b)

Figure 3: MCRB vs. normalized timing variance with $N = 4$ for (a) MIL-STD SOQPSK and (b) SOQPSK-TG.

result holds for both versions of SOQPSK and rules out the existence of false-lock points. The constant k_p is defined as the slope of the S-curve evaluated at $\delta = 0$ and the value of k_p is determined numerically via simulation. The values of k_p measured numerically agree with the values given in [18].

The relationship between the observation interval L_0 in a feedforward-based scheme and the normalized loop bandwidth BT_s in a feedback-based scheme is [18]

$$L_0 T_s = \frac{1}{2BT_s}.$$

The accuracy of the feedback scheme is measured numerically via simulation with the *normalized timing variance*

$$\frac{1}{T_s^2} \times \sigma_\tau^2 \triangleq \frac{1}{T_s^2} \times \text{Var}\left\{\hat{\tau}[k] - \tau\right\}. \tag{22}$$

In this paper, the timing variance has been computed for two different values of the normalized loop bandwidth, for both versions of SOQPSK (a total of four cases). Fig. 3 shows the normalized timing variances plotted along with their corresponding MCRB(τ)'s. All four cases reveal that the TED is very effective for SOQPSK, since the normalized timing variance is quite close to the lower performance limit indicated by MCRB(τ).

These synchronization results further validate the CPM model for SOQPSK, which has already proven effective in detection algorithms. Moreover, in the case of SOQPSK-TG where the reduced-complexity pulse truncation approximation is used, it is especially pleasing that such low values of the timing variance are achieved using the suboptimal MF output samples. The proposed TED shows a marked improvement in performance when compared to the *non data aided* TED developed very recently in [19] for SOQPSK. In particular, the TED presented here allows for much wider loop bandwidths and the rapid synchronization times that result.

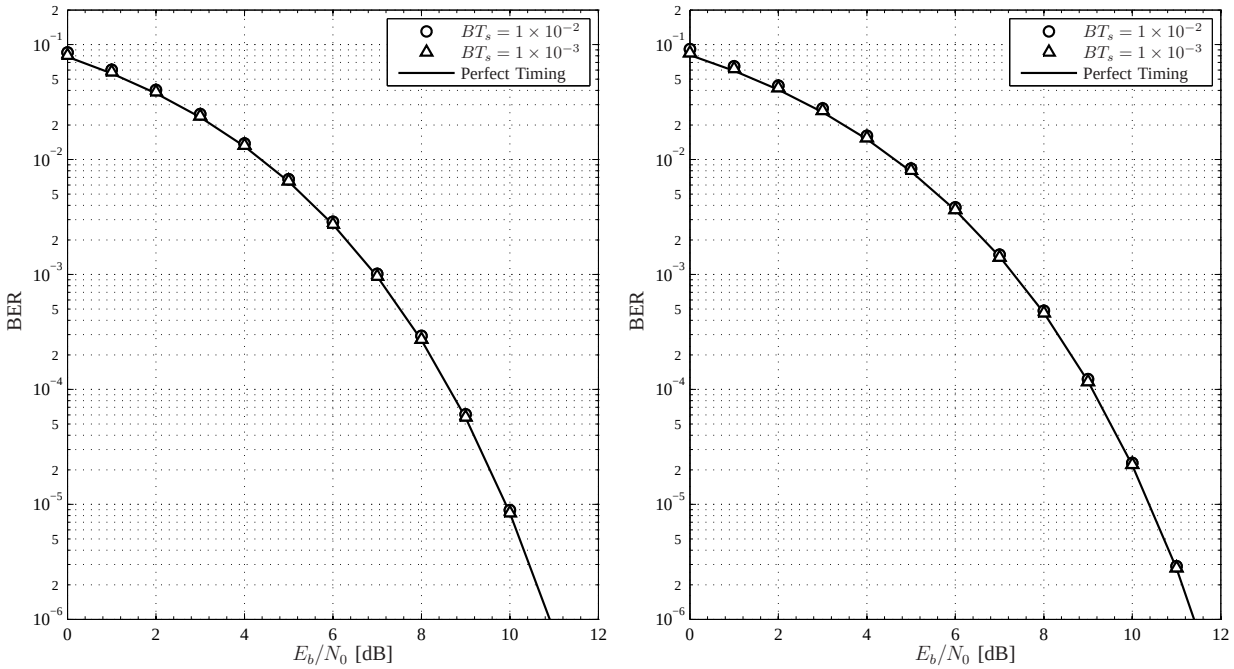

(a) (b)

Figure 4: Probability of bit error for (a) MIL-STD SOQPSK and (b) SOQPSK-TG.

Fig. 4 quantifies the bit error rate (BER) performances of the proposed TED for MIL-STD SOQPSK and SOQPSK-TG. The theoretical performance of the optimal MIL-STD SOQPSK detector with perfect symbol timing is given in [6]. This ideal performance curve is shown in Fig. 4 along with the simulated results for the bit error performance of the TED with $BT_s = 1 \times 10^{-3}$ and $BT_s = 1 \times 10^{-2}$. It can be seen that the detector performs at the theoretical limit, with the simulation points perfectly lining up over the analytical curve. The fact that this performance is achieved with the wider loop bandwidth of $BT_s = 1 \times 10^{-2}$ is noteworthy.

Similarly, the theoretical performance of SOQPSK-TG with the 4-state pulse truncation approximation and perfect symbol timing is given in [11]. As in the previous case, the TED provides accurate results even with $BT_s = 1 \times 10^{-2}$. This demonstrates the applicability of the TED to both versions of SOQPSK, which is significant since the *non data-aided* TED in [19] has extremely poor performance in the case of SOQPSK-TG.

VI. CONCLUSION

We have shown that an existing TED for CPM can be extended to SOQPSK where the data symbols have a constrained ternary data alphabet and reduced-complexity suboptimal detectors are required. This timing recovery scheme is of practical significance since SOQPSK is widely used in military and aeronautical telemetry. Moreover, optimal CPM-based detectors have only recently been proposed for SOPQSK and compatible timing recovery schemes, such as the one proposed here, are required for these detectors to be implemented in practice.

Unlike another TED recently developed for SOQPSK, the performance of the TED proposed here is exceptionally good in terms of approaching the theoretical lower bounds on timing error variance estab-

lished by the MCRB. Furthermore, the bit error performance of the detector was identical to the perfect timing case, even when reasonably large values of the loop bandwidth were used. Based on these results, the proposed scheme has potential in a wide range of applications due to its low complexity, its lack of false lock points and fast acquisition capabilities.

REFERENCES

[1] J. B. Anderson, T. Aulin, and C.-E. Sundberg, *Digital Phase Modulation*. New York: Plenum Press, 1986.

[2] D. I. S. Agency, "Department of Defense interface standard, interoperability standard for single-access 5-kHz and 25-kHz UHF satellite communications channels." Tech. Rep. MIL-STD-188-181B, Department of Defense, Mar. 1999.

[3] Range Commanders Council Telemetry Group, Range Commanders Council, White Sands Missile Range, New Mexico, *IRIG Standard 106-00: Telemetry Standards*, 2000. (Available on-line at http://www.ntia.doc.gov/osmhome/106.pdf).

[4] T. Hill, "A non-proprietary, constant envelope, variant of shaped offset QPSK (SOQPSK) for improved spectral containment and detection efficiency," in *Proc. IEEE MILCOM*, Oct. 2000.

[5] L. Li and M. Simon, "Performance of coded OQPSK and MIL-STD SOQPSK with iterative decoding," *IEEE Trans. Commun.*, vol. 52, pp. 1890–1900, Nov. 2004.

[6] E. Perrins and M. Rice, "Simple detectors for shaped-offset QPSK using the PAM decomposition," in *Proc. IEEE Global Telecommunications Conf.*, (St. Louis, Missouri), pp. 408–412, Nov./Dec. 2005.

[7] P. A. Laurent, "Exact and approximate construction of digital phase modulations by superposition of amplitude modulated pulses (AMP)," *IEEE Trans. Commun.*, vol. 34, pp. 150–160, Feb. 1986.

[8] E. Perrins and M. Rice, "PAM representation of ternary CPM." Submitted to *IEEE Transactions on Communications*, Mar. 2005. See also: E. Perrins and M. Rice, "PAM Representation of Ternary Continuous Phase Modulation," *Department of Electrical and Computer Engineering*, Brigham Young University, Feb. 2005. [Online]. Available: https://dspace.byu.edu/handle/1877/58.

[9] T. Aulin, C.-E. Sundberg, and A. Svensson, "Viterbi detectors with reduced complexity for partial response continuous phase modulation," in *Proc. National Telecommun. Conf., NTC'81*, (New Orleans, LA), pp. A7.6.1–A7.6.7, Nov./Dec. 1981.

[10] A. Svensson, C.-E. Sundberg, and T. Aulin, "A class of reduced-complexity Viterbi detectors for partial response continuous phase modulation," *IEEE Trans. Commun.*, vol. 32, pp. 1079–1087, Oct. 1984.

[11] E. Perrins and M. Rice, "A reduced-complexity approach to iterative detection of SOQPSK," to be published in *IEEE Trans. Commun.*, July 2007.

[12] G. Colavolpe and R. Raheli, "Noncoherent sequence detection of continuous phase modulations," *IEEE Trans. Commun.*, vol. 47, pp. 1303–1307, Sept. 1999.

[13] M. Morelli, U. Mengali, and G. M. Vitetta, "Joint phase and timing recovery with CPM signals," *IEEE Trans. Commun.*, vol. 45, pp. 867–876, July 1997.

[14] M. Simon, *Bandwidth-Efficient Digital Modulation With Application to Deep-Space Communication*. New York: Wiley, 2003.

[15] M. J. Dapper and T. J. Hill, "SBPSK: A robust bandwidth-efficient modulation for hard-limited channels," in *Proc. IEEE MILCOM*, Oct. 1984.

[16] M. K. Simon, "Multiple-bit differential detection of offset QPSK," *IEEE Trans. Commun.*, vol. 51, pp. 1004–1011, June 2003.

[17] A. N. D'Andrea, U. Mengali, and R. Reggiannini, "The modified Cramer-Rao bound and its application to synchronization problems," *IEEE Trans. Commun.*, vol. 42, pp. 1391–1399, Feb./Mar./Apr. 1994.

[18] U. Mengali and A. N. D'Andrea, *Synchronization Techniques for Digital Receivers*. New York: Plenum Press, 1997.

[19] P. Chandran, "Symbol timing recovery for SOQPSK," Master's thesis, University of Kansas, Lawrence, Kansas, 2007.